Materials Today Communications 45 (2025) 111977

Contents lists available at ScienceDirect

Materials Today Communications

journal homepage: www.elsevier.com/locate/mtcomm

High temperature compression tests for liquid metal embrittlement characterisation in steels

L. Ripperger [a,*], T. Burlet [a], K.D. Molodov [b], S. Sandlöbes-Haut [a]

[a] RWTH Aachen University, Institute of Physical Metallurgy and Materials Physics, Kopernikusstrasse 14, 52074 Aachen, Germany
[b] Department of New Materials and Technologies, Salzgitter Mannesmann Forschung GmbH, Eisenhüttenstr. 99, 38239 Salzgitter, Germany

ARTICLE INFO

Keywords:
Advanced high strength steel
Galvanising
Liquid metal embrittlement
Welding process

ABSTRACT

A method was developed to investigate Zn-induced liquid metal embrittlement under simultaneous action of compressive stress and elevated temperature to simulate key aspects of the conditions that occur during resistance spot welding of steel sheet. We demonstrate the capability of the experimental set-up to analyse microstructural changes and phase transitions in the base substrate on the example of a medium Mn steel in combination with Zn. Major advantages of the testing methodology are high heating rates achieved through inductive heating and the application of a simplified compressive stress-state resembling key characteristics of spot welding conditions, i.e. indenting into the material as opposed to tensile testing. Furthermore, the method allows for post-mortem investigations and characterisation of Zn-enriched intermediate layers via specially prepared cross-sections on the mesoscale. This methodology was used to demonstrate that there were no notable changes in the reference material (IF steel) upon application of stress and temperature, whereas the medium Mn steel exhibited the formation of an intermediate layer at the liquid/solid interface, which constitutes an important mechanism with respect to liquid metal embrittlement.

The methodology developed aims at unravelling the complicated influence of the stress-state and temperature during resistance spot welding under well-defined laboratory conditions by varying the Zn coating, temperature, and load independently, thus providing a means to uncover the fundamental mechanism of liquid metal embrittlement.

Contents

* Corresponding author.
E-mail address: ripperger@imm.rwth-aachen.de (L. Ripperger).

https://doi.org/10.1016/j.mtcomm.2025.111977
Received 12 November 2024; Received in revised form 13 February 2025; Accepted 19 February 2025
Available online 8 March 2025

1. Introduction

In recent years, advanced high-strength steels (AHSS) have become increasingly important for the design of lightweight automotive parts, owing to increasing demands on improved formability and energy-absorbing properties. These steels contain in many cases manganese (Mn), which not only enables the formation of complex and multiphase microstructures with increased strength and ductility but also facilitates weight reduction through increased strength [1–3]. Due to the higher strength of Mn steels, thinner and lighter components can be produced without compromising structural integrity, contributing to the vehicle's weight reduction, which leads to better fuel efficiency and reduced emissions.

An efficient way to protect steels against corrosion is coating with Zn [4–6]. Since the 1930s, resistance spot welding (RSW) has been used as one of the preferred methods to join the parts of e.g. car bodies. During RSW heat is locally introduced and causes melting of the material to join the parts in the form of a spot weld [7–12].

During RSW, especially at increased current and welding times, some galvanised high-strength steel grades can be prone to cracking at the shoulders and at the centre of the weld spots that affect the crash-worthiness of the component [13–19]. The formation of shoulder cracks is known to be caused by liquid metal embrittlement (LME), where it has been reported that the simultaneous action of stress, temperature and a liquid metal (e.g. Zn) are prerequisites for the occurrence of LME [20]. Zn-induced LME typically leads to cracking at the shoulders of the weldment, where both tensile and compressive stresses are present. In contrast, the weld centre is primarily affected by Cu-induced embrittlement originating from contact to the electrode rather than Zn-induced LME. This is characterised by local embrittlement, i.e. a loss in elongation and ultimate tensile strength which occurs over a range of temperatures and strain rates, due to rapid penetration of the liquid metal into the microstructure along the grain boundaries [21–25].

In the last decade, grain boundary penetration, wetting and LME have been observed in various solid/liquid material combinations, including Zn-induced LME in galvanised steels [22,26–28]. However, mainly twinning induced plasticity (TWIP) and transformation induced plasticity (TRIP) steels with higher Mn contents were investigated using high temperature tensile tests and welding tests. The number of investigations on the effect of liquid Zn on medium Mn steels is up-to date limited and further studies are necessary to understand the underlying mechanisms that are causing embrittlement in these multiphase microstructures comprising a significant fraction of austenite in an effort to combat the effect of LME.

The focus of this work is to design an experimental set-up that allows to systematically vary the major influencing factors, inter alia, the Zn coating, time, temperature, and load independently in order to study Zn-induced LME on a laboratory scale. Further, the developed methodology is used to compare a medium Mn steel with a reference (IF) steel. The effects of Zn, temperature and load were investigated using scanning electron microscopy (SEM) and energy-dispersive X-ray spectroscopy (EDS).

2. Experimental procedure

2.1. Materials

To investigate the influence of Zn-induced LME, a medium Mn steel with the composition Fe-0.05%C-12%Mn-3%Al in wt.-% and an austenite content of about 40% was investigated [29–31]. Instead of galvanising, a Zn (4N5) foil with 0.1 mm thickness was used to simulate the Zn coating. The medium Mn steel was cut into cylinders with a height of 4 mm and a diameter of 7 mm using electric discharge machining (EDM). The surface layer that might be contaminated with copper (Cu) (due to electric discharge erosion) was removed since Cu can also cause embrittlement of steels [32–36]. Furthermore, a purely ferritic, industrially produced hot-dip galvanised IF steel supplied by Salzgitter AG was investigated as a reference, where LME is not expected to be observable. Due to the galvanised sheet provided, the cylinder height was 1 mm with a constant diameter of 7 mm.

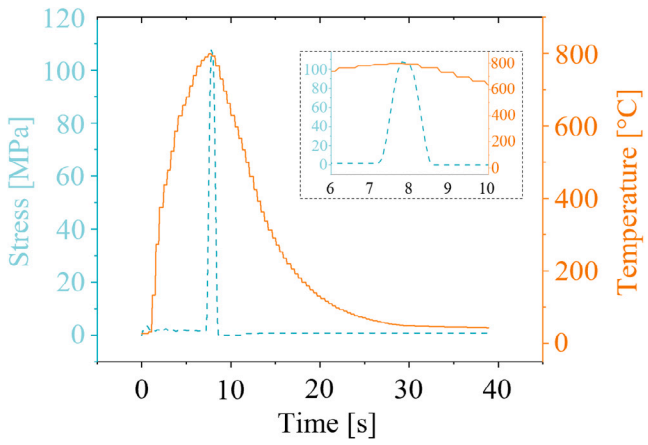

Fig. 1. Load and temperature curves over time during the compression test of Fe-0.05wt.-%C-12wt.-%Mn-3wt.-%Al steel, with a magnified view of the critical period between 6 and 10 s. The experimental set-up enables the application of a short load impulse within seconds upon reaching the desired temperature.

2.2. Experimental set-up and testing procedure

The custom test set-up was built on a Zwick Roell 1484 testing machine. It enables high-temperature compression tests with inductive heating, capable of reaching temperatures exceeding 800 °C. The experiments were performed at 800 °C, with a heating rate of 109 K s^{-1}. The set-up enables the simultaneous application of compressive stresses of up to 10 kN and high temperatures, thereby providing an approach to simulate some aspects of the resistance spot welding process under well-defined and controlled laboratory conditions. A notable feature of the set-up is the use of compressive stresses as opposed to a tensile stress-state, e.g. as in hot tensile testing using a Gleeble thermomechanical simulator, which is commonly used to access the effect of LME [37]. However, it should be noted that while RSW induces a complex three-dimensional stress state, the applied compression test represents a more idealised stress condition. This approach enables a controlled variation of stress, temperature, and Zn interaction while facilitating future modelling approaches such as crystal plasticity or phase-field simulations, which are more challenging under indentation-like stress conditions.

To simulate the welding process and avoid evaporation of the Zn, the Zn foil was placed between two steel cylinders (each with a height of 4 mm). This "sandwich" was stacked between two ceramic stamps in the Zwick-Roell testing machine and clamped with a compressive pre-load of 100 N (2.6 MPa based on the sample geometry) to prevent the sample-sandwich from slipping away.

An induction coil was placed around the sample-sandwich to ensure homogeneous heating of the samples. In order to ensure accurate monitoring of the sample temperature, a thermocouple was embedded at the centre of the sample, thus ensuring direct contact between the bimetal junction and the specimen. In the automated mode, the experiment is temperature-controlled: when a temperature of 800 °C was reached, the machine compressed the sample with the set load for a duration of less than a second, immediately followed by quenching the sample to room temperature with compressed air, while sustaining a force of 50 N. That said, it is possible to individually adjust temperature and load up to 800 °C and up to 10 kN, respectively. Fig. 1 shows an exemplary temperature-load curve and Fig. 2 depicts the experimental set-up.

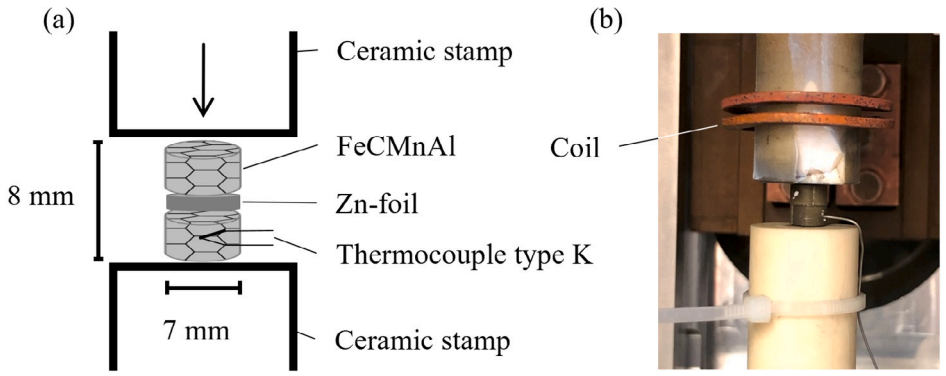

Fig. 2. (a) Schematic of the experimental set-up of the high temperature compression test on a Zwick Roell 1484 at temperatures of 800 °C and forces of 100 MPa using the example of Fe-0.05wt.-%C-12wt.-%Mn-3wt.-%Al steel and (b) photograph of the respective set-up. During the experiment, the coil is placed around the sample.

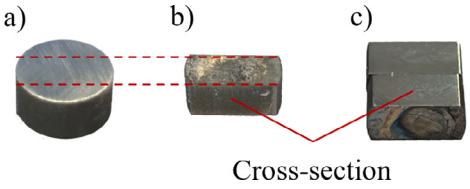

Fig. 3. Sample preparation steps of Fe-0.05wt.-%C-12wt.-%Mn-3wt.-%Al steel: (a) cylindrical sample with ground surface before the compression test (red dashed line indicates the cutting line), (b) cut samples after the test, with the cross-section still showing the spark-erosive contaminated layer, and (c) two samples glued together with the cross-sections facing upwards after the final polishing step with OPS.

2.3. Sample preparation

To characterise the relevant area of the samples using SEM and EDS, i.e. the surface normal to the compression direction, a sharp edge is needed on the surface within the sample's cross-section. To ensure this, both halves of the sandwich sample were separated along their mutual solidified zinc layer and transversely cut using EDM after testing (Fig. 3). Subsequently, the two cut samples were fixed on a holder with the cross-sectional surfaces facing upwards, ensuring that the Zn-coated surfaces were in contact with each other to avoid contamination of the near-surface areas.

To produce sharp edges the samples were then grinded up to a grit size of 4000 and polished using a diamond suspension down to a particle size of 0.25 μm. The final step of the metallographic preparation comprised polishing using an oxide polishing suspension (OPS) for 50 s, followed by cleaning. After the preparation, the samples were mounted on a (SEM) stub using silver adhesive and analysed using a SEM (Helios Nanolab 600i, FEI Inc.).

3. Results and discussion

The experiments were performed at a temperature of 800 °C and an initial strain rate of $>10^{-2}$ s^{-1} based on investigations by Beal et al. Jung et al. and Kang et al. [38–40] who showed the appearance of LME in galvanised high Mn steels at high strain rates and temperatures above 700 °C. Furthermore, according to Beal et al. stresses slightly above the yield stress are necessary for Zn-induced LME [38]. Based on preliminary investigations on the medium Mn steel, an approximate yield strength ($R_{p0.2}$) of 100 MPa can be assumed at 800 °C [29–31], which was applied as a compressive load in the experiments. The initial strain rate allowed to reach the required stresses within one second.

Based on these parameters, we systematically varied (i) presence of Zn, (ii) temperature, (iii) load, and analysed the microstructure of surface-near sample areas with a special focus on indications for LME.

3.1. Influence of Zinc

First, experiments were performed without the presence of Zn to distinguish microstructural features of the near-surface areas that occur in the presence of Zn only. The analysis of SEM micrographs of the surface cross-section of the medium Mn steel after compression at 800 °C with stresses of 100 MPa and 160 MPa, respectively, showed no cracks or any evidence of material embrittlement. No significant difference was observed between samples compressed with 100 MPa and 160 MPa, indicating that a variation of the compressive load within this range does not affect the surface/interface characteristics.

3.1.1. Zinc and temperature

Heating a medium Mn sample-sandwich containing a Zn-layer to 800 °C for a short period (without applied stress) causes melting of the Zn layer, resulting in a noticeable alteration of the material's surface/interface characteristics, Fig. 4. The SEM micrograph reveals a porous layer on top of the bulk material, due to the molten and resolidified Zn (denoted by (i) in Fig. 4). Below this top layer is an intermediate layer that is compact (i.e. less porous) but comparatively coarse-grained with the bulk material located just underneath (inset in the SE image in Fig. 4). EDS measurements showed that the top porous layer was not only rich in Zn (60–80 at.-%), but also contained iron (Fe) (10–20 at.-%) and small amounts of aluminium (Al). The intermediate layer ((ii) in Fig. 4) was composed of Fe, Zn and Al, while the bulk region ((iii) in Fig. 4) remained unchanged and no diffusion of Zn into the bulk or penetration of the grain boundaries with Zn were evident.

Fig. 5 shows an electron backscatter diffraction (EBSD) phase map of the galvanised steel sample and illustrates the microstructural changes in the near-surface region. A thin austenitic layer can be seen below the coarse-grained intermediate layer, indicating that the influence of temperature and the resulting liquid zinc is sufficient to induce a phase transformation in the steel. However, the layers appear thicker in the EBSD image than in the EDS and SE images. This discrepancy is due to the 70 °C tilt required for EBSD imaging, which, despite tilt correction, introduces geometric distortion that makes the layers appear thicker than in the 0 °C EDS images.

The exact composition of the intermediate layer was difficult to determine due to its relatively small size compared to the huge EDS interaction volume of about 1 μm in bulk materials. Further investigations using EDS on thin foils or atom probe tomography (APT) are required to quantitatively measure the composition of the intermediate and austenitic layer with higher accuracy. In any case, the analysis showed that the Zn does not form a pure Zn layer on top of the material, but that Fe and Al dissolved into the most-top Zn layer, leading to the formation of an intermediate layer even in the absence of applied stress, presumably due to Zn diffusion into the bulk. In addition, no Zn penetration along grain boundaries was observed, indicating that the simultaneous action of temperature and stress is required to induce

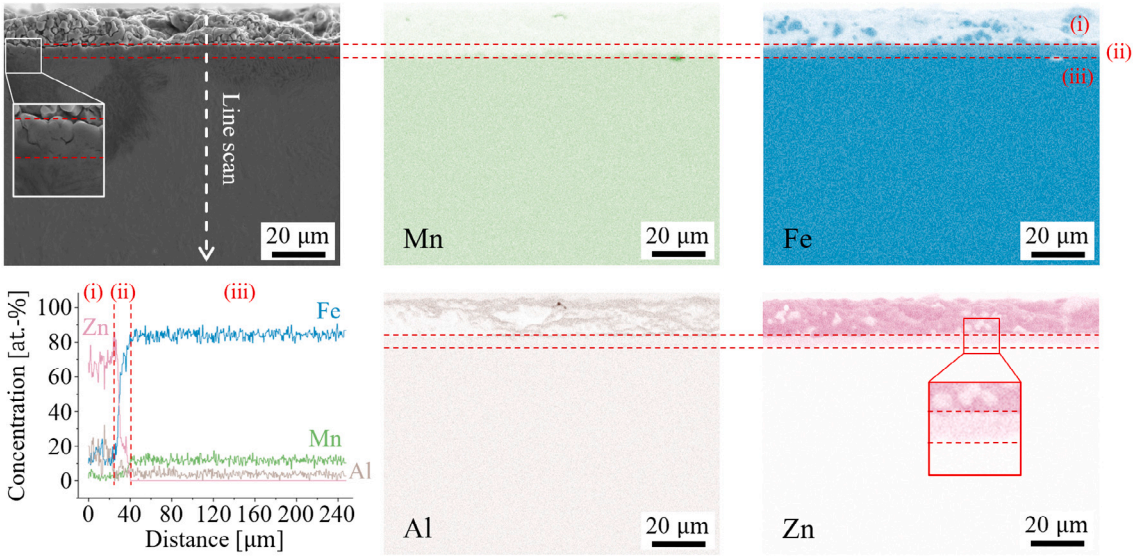

Fig. 4. EDS images and line scan in at.-% of galvanised Fe-0.05wt.-%C-12wt.-%Mn-3wt.-%Al steel samples after heat treatment at 800 °C with a Zn-rich layer (i), intermediate layer (ii) and bulk material (iii). The inset in the SE image and Zn EDS map depicts an enlarged view of the intermediate layer.

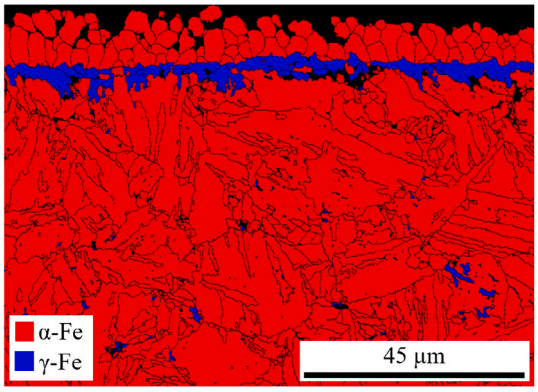

Fig. 5. EBSD phase Map of galvanised Fe-0.05wt.-%C-12wt.-%Mn-3wt.-%Al steel sample after heat treatment at 800 °C indicating BCC and FCC phase.

LME. In addition, the intermediate layer in the medium Mn steel contains significant amounts of Al, and the Fe-Zn-Al phase diagram suggests that no intermetallic phases are expected at 800 °C. Instead, the formation of α-Fe with Zn and Al incorporation is likely, explaining the deviation from the intermetallic phases predicted in the binary Fe-Zn system.

3.1.2. Zinc, temperature and stress

Subsequent experiments were conducted with applied stress on sample-sandwiches comprising two cylinders of medium Mn steel with a Zn foil placed between them. The compression tests of these sample-sandwiches were performed at 800 °C under stresses of 100 MPa (approximate yield stress at 800 °C), 160 MPa, 180 MPa and 200 MPa. Fig. 6 shows corresponding SE images of the surface-near region of the compressed sample-sandwiches. At 800 °C and a stress of 100 MPa, a porous surface layer and an intermediate layer formed above the bulk material (Fig. 6a), as observed previously without the application of stress. From the micrographs, it appears that there is no significant difference in the intermediate layer formed during compression at stresses of 100–200 MPa (the top-most layer could not be preserved during metallographic samples preparation of the samples compressed at 160 MPa, 180 MPa and 200 MPa). However, compared to the tests without applied stress, the intermediate layers were much thicker in all compressed samples. Further analysis using EDS was performed on the sample compressed at 100 MPa (Fig. 6a).

Fig. 7 presents EDS maps and line scans of the sample compressed at 100 MPa and 800 °C in the presence of Zn. The analysis confirms that the intermediate layer, which was less than 4 µm thick in the unstressed sample, had increased to about 15-20 µm in the compressed sample. While the intermediate layer appears relatively compact in the uncompressed sample, in the compressed sample, the regions between the newly formed coarse grains exhibit porosity and extend into the top-most Zn-rich layer. The composition of the top-most layers was similar in the compressed and uncompressed samples containing about 70–75 at.-%, Zn between 20–25 at.-%, and Al up to 5 at.-%. The intermediate layer in the compressed sample was rich in Fe (~70 at.-%) and contained Zn (~20–25 at.-%), enriched with Al when compared to the bulk matrix and contained small amounts of Mn. Zn was segregated in the intergrain regions of this intermediate layer. No Zn diffusion into the bulk material was evident from the EDS measurement.

Such a coarse-grained layer with Zn-enriched intergrain regions has been observed in high Mn, TRIP, and TWIP steels [15,40–43], suggesting that the experimental set-up developed in the present study is able to reproduce the processes and mechanisms acting during RSW of Zn-coated materials.

3.1.3. IF steel

For reference, experiments were conducted on an industrially produced galvanised IF steel supplied by Salzgitter AG that is not sensitive to LME [40]. Due to the lower yield strength of the IF steel at 800 °C the plastic deformation of the surface layer was significantly higher than in the medium Mn steel, Fig. 8a. The formation of a Fe-Zn layer was not observed in the IF steel, Fig. 8. Penetration of Zn along grain boundaries or cracking was not evidenced.

3.2. Final discussion

During compression of the medium Mn steel in contact with Zn at 800 °C slightly above the yield strength ($R_{p0.2}$) a Fe-Zn intermediate layer formed in between the Zn-rich top layer and the bulk material. This layer was enriched in Al with respect to the matrix composition and contained small amounts of Mn. The thickness of this layer amounted to 15-20 µm and the intergrain regions were enriched in Zn. It is important to note that, although the porous nature of this intermediate layer might initially be mistaken for cracking of the base

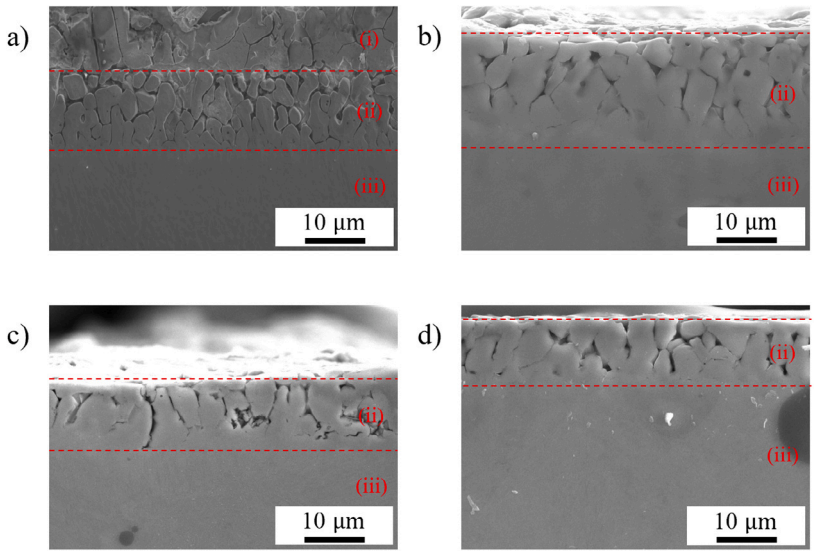

Fig. 6. SE images of the Fe-0.05wt.-%C-12wt.-%Mn-3wt.-%Al steel sample with Zn pressed at 800 °C and different stresses; (a) 100 MPa, (b) 160 MPa, (c) 180 MPa, (d) 200 MPa with Zn-rich layer (i), intermediate layer (ii) and bulk material (iii).

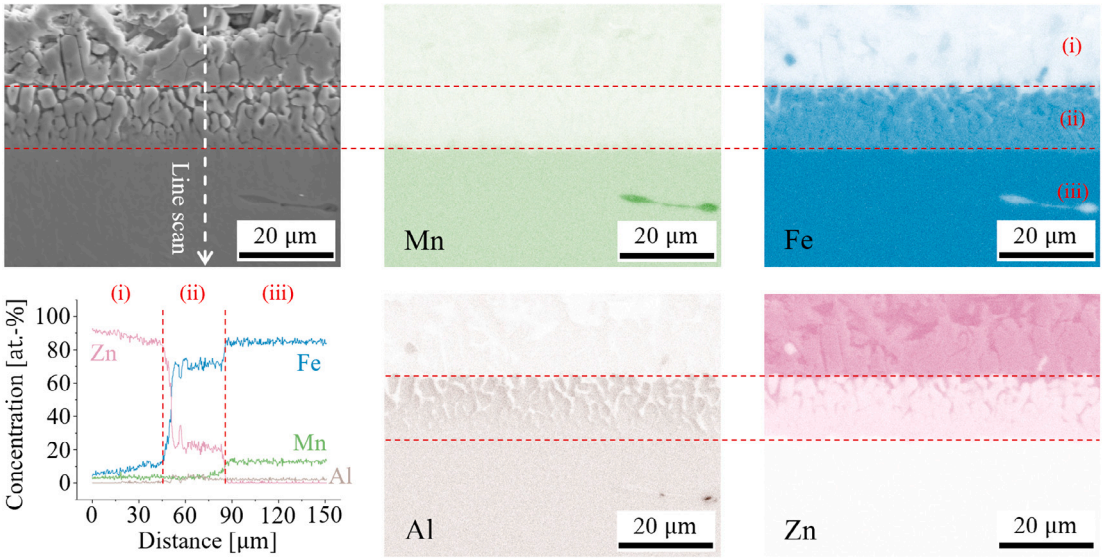

Fig. 7. EDS images and line scan in at.-% of galvanised Fe-0.05wt.-%C-12wt.-%Mn-3wt.-%Al steel samples after the experiment at 800 °C and 100 MPa with Zn-rich layer (i), intermediate layer (ii) and bulk material (iii).

substrate, detailed analysis did not reveal any evidence of cracking in the base steel or Zn penetration into the grain boundaries of the bulk material, causing LME. When the same medium Mn steel was brought into contact with Zn and heated to 800 °C without applying compressive stress, a similar intermediate layer formed, however, significantly more compact/less porous and thinner (less than 4 µm) and without any Zn enrichment in the intergrain regions/grain boundaries. The small amounts of Mn detected in this intermediate layer indicates that the layer formed from dissolution of the bulk material, as solid diffusion of Mn is very slow [44], hence Mn will not diffuse over several µm during the short time of the experiment. In both experiments the top Zn-rich layer contained about 20 at.-% Fe and small amounts of Al, indicating the diffusion of Fe and Al from the matrix into the liquid Zn.

Similar intermediate layers, as evidenced in the current experiment, were observed in the case of high Mn TRIP and TWIP steels [15,40–43], indicating that such layers can form not only in austenitic-martensitic Mn steels, but also in purely austenitic Mn steels. In any case, intermediate layers that impede direct wetting of the bulk substrate and grain boundaries by liquid Zn can be thought of as aiding in the prevention of LME. It is noteworthy, that the (ferritic) IF reference steel in the present study did not form such an intermediate layer. The exact mechanism of the formation of the intermediate layer and its mechanistic importance for the prevention of LME will be discussed in detail elsewhere [45].

4. Conclusion

In this work, high temperature compression tests were conducted on a medium Mn steel in the presence of Zn. The aim of this study was to develop and validate a new experimental method to study Zn-induced LME on the laboratory scale with independent control of temperature, stress, base alloy and coating. In summary, the following conclusions can be drawn:

- A novel method was successfully developed to simulate the conditions of resistance spot welding by applying compressive stress and elevated temperature, providing a reliable approach to investigate Zn-induced LME.

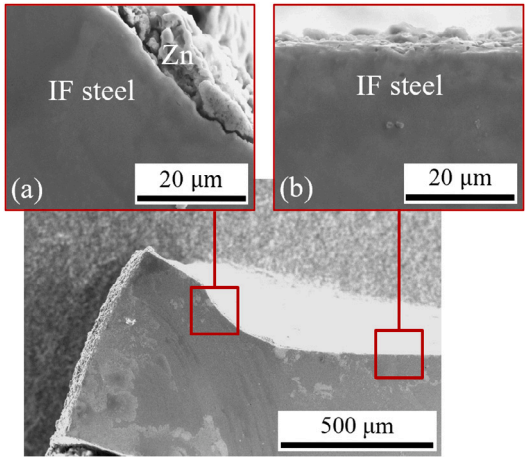

Fig. 8. IF steel sample after compression testing with Zn at 800 °C and 127 MPa; (a) High deformed region and (b) less deformed area.

- The methodology allows the high-resolution analysis of changes at the liquid/solid interface and relevant phase transitions within the bulk material, which are critical to understanding the LME process.
- The use of inductive heating enables high heating rates of the order of 10^2 K s^{-1}, and the application of a stress-state that approximates spot welding conditions and offers additional insights compared to traditional tensile testing methods.
- Post-mortem investigations were showcased that allow, detailed characterisation of Zn-rich layers through specially prepared cross-sections, which is essential for understanding the effects of LME on the micro- and mesoscale.
- Initial findings indicate that while the reference IF steel displayed no significant microstructural changes in the vicinity of the liquid/solid interface, in the medium Mn steel a coarse and porous intermediate layer between the Zn-rich surface layer and the bulk layer formed, suggesting that it might play a crucial role for prevention of LME.

Overall, the developed method proves to be a powerful tool for simulating and studying LME in steels, with the added advantage of independently varying the base alloy, Zn coating, temperature, and load. This approach offers a controlled and systematic way to unravel the fundamental mechanisms involved in LME.

CRediT authorship contribution statement

L. Ripperger: Writing – review & editing, Writing – original draft, Visualization, Methodology, Investigation, Formal analysis, Data curation, Conceptualization. **T. Burlet:** Software, Methodology. **K.D. Molodov:** Writing – review & editing, Visualization, Validation, Resources, Methodology, Investigation, Conceptualization. **S. Sandlöbes-Haut:** Writing – review & editing, Visualization, Validation, Supervision, Resources, Project administration, Methodology, Funding acquisition, Formal analysis, Conceptualization.

Declaration of competing interest

The authors declare that they have no known competing financial interests or personal relationships that could have appeared to influence the work reported in this paper.

Acknowledgements

The authors gratefully acknowledge the German Research Foundation (DFG) for support of SFB 761 (project number: 29898171), Transferproject T7. Fruitful discussions with Dr. Tilmann Hickel (BAM, MPIE) and Dr. Ujjal Saikia (MPIE) are acknowledged.

Data availability

Data will be made available on request.

References

[1] B.C. De Cooman, Y. Estrin, S.K. Kim, Twinning-induced plasticity (TWIP) steels, Acta Mater. 142 (2018) 283–362.
[2] D. Raabe, H. Springer, I. Gutiérrez-Urrutia, F. Roters, M. Bausch, J.B. Seol, M. Koyama, P.P. Choi, K. Tsuzaki, Alloy design, combinatorial synthesis, and microstructure–property relations for low-density Fe-Mn-Al-C austenitic steels, Jom 66 (2014) 1845–1856.
[3] H. Springer, D. Raabe, Rapid alloy prototyping: Compositional and thermo-mechanical high throughput bulk combinatorial design of structural materials based on the example of 30Mn–1.2 C–xAl triplex steels, Acta Mater. 60 (12) (2012) 4950–4959.
[4] Y. Kim, J. Lee, J. Park, S.-H. Jeon, Effect of Si content on wettability of dual phase high strength steels by liquid Zn-0.23 wt.% Al, Met. Mater. Int. 17 (2011) 607–611.
[5] A.R. Marder, The metallurgy of zinc-coated steel, Prog. Mater. Sci. 45 (3) (2000) 191–271.
[6] M.-S. Oh, S.-H. Kim, J.-S. Kim, J.-W. Lee, J.-H. Shon, Y.-S. Jin, Surface and cut-edge corrosion behavior of Zn-Mg-Al alloy-coated steel sheets as a function of the alloy coating microstructure, Met. Mater. Int. 22 (2016) 26–33.
[7] A. Al-Mukhtar, Review of resistance spot welding sheets: processes and failure mode, in: Advanced Engineering Forum, Vol. 17, Trans Tech Publ, 2016, pp. 31–57.
[8] A. Al-Mukhtar, Q. Doos, The spot weldability of carbon steel sheet, Adv. Mater. Sci. Eng. 2013 (1) (2013) 146896.
[9] D. Dickinson, Welding in the Automotive Industry: State of the Art, Republic Steel Research Center, 1981.
[10] H. Moshayedi, I. Sattari-Far, Numerical and experimental study of nugget size growth in resistance spot welding of austenitic stainless steels, J. Mater. Process. Technol. 212 (2) (2012) 347–354.
[11] N. Williams, J. Parker, Review of resistance spot welding of steel sheets Part 1 Modelling and control of weld nugget formation, Int. Mater. Rev. 49 (2) (2004) 45–75.
[12] N. Williams, J. Parker, Review of resistance spot welding of steel sheets Part 2 Factors influencing electrode life, Int. Mater. Rev. 49 (2) (2004) 77–108.
[13] C.-W. Ji, I. Choi, Y.D. Kim, Y.-D. Park, Study on coating melting behavior on weld growth mechanism for Al-Si coated hot-stamped boron steels in resistance spot welding, Korean J. Metals Mater. 52 (11) (2014) 931–941.
[14] Y.G. Kim, I.J. Kim, J.S. Kim, Y.I. Chung, Y.C. Du, Evaluation of surface crack in resistance spot welds of Zn-coated steel, Mater. Trans. 55 (1) (2014) 171–175.
[15] C.W. Lee, D.W. Fan, I.R. Sohn, S.-J. Lee, B.C. De Cooman, Liquid-metal-induced embrittlement of Zn-coated hot stamping steel, Met. Mater. Trans. A 43 (2012) 5122–5127.
[16] H. Gaul, G. Weber, M. Rethmeier, Influence of HAZ cracks on fatigue resistance of resistance spot welded joints made of advanced high strength steels, Sci. Technol. Weld. Join. 16 (5) (2011) 440–445.
[17] M. Milititsky, E. Pakalnins, C. Jiang, A.K. Thompson, On characteristics of DP600 resistance spot welds, SAE Trans. (2003) 244–251.
[18] D. Sigler, J. Schroth, W. Yang, X. Gayden, C. Jiang, Y. Sang, P. Morin, Observations of liquid metal-assisted cracking in resistance spot welds of zinc-coated advanced high-strength steels, in: Sheet Metal Welding Conference Sheet Metal Welding Conf. XIII, 2008.
[19] B. Yan, H. Zhu, S. Lalam, S. Baczkowski, T. Coon, Spot Weld Fatigue of Dual Phase Steels, SAE Technical Paper, 2004.
[20] M. Nicholas, C. Old, Liquid metal embrittlement, J. Mater. Sci. 14 (1979) 1–18.
[21] P. Fernandes, D. Jones, Specificity in liquid metal induced embrittlement, Eng. Fail. Anal. 3 (1996).
[22] B. Joseph, M. Picat, F. Barbier, Liquid metal embrittlement: A state-of-the-art appraisal, Eur. Phys. J.- Appl. Phys. 5 (1) (1999) 19–31.
[23] B. Joseph, F. Barbier, M. Aucouturier, Embrittlement of copper by liquid bismuth, Scr. Mater. 40 (8) (1999) 893–897.
[24] P. Fernandes, D. Jones, The effects of microstructure on crack initiation in liquid-metal environments, Eng. Fail. Anal. 4 (3) (1997) 195–204.
[25] A. Legris, G. Nicaise, J.-B. Vogt, J. Foct, D. Gorse, D. Vançon, Embrittlement of a martensitic steel by liquid lead, Scr. Mater. 43 (11) (2000) 997–1001.

[26] R. Hugo, R. Hoagland, In-situ TEM observation of aluminum embrittlement by liquid gallium, Scr. Mater. 38 (3) (1998) 523–529.
[27] B. Joseph, F. Barbier, G. Dagoury, M. Aucouturier, Rapid penetration of liquid Bi along Cu grain boundaries, Scr. Mater. 39 (6) (1998) 775–781.
[28] W. Ludwig, E. Pereiro-López, D. Bellet, In situ investigation of liquid Ga penetration in Al bicrystal grain boundaries: grain boundary wetting or liquid metal embrittlement? Acta Mater. 53 (1) (2005) 151–162.
[29] A. Dutta, D. Ponge, S. Sandlöbes, D. Raabe, Understanding hot vs. cold rolled medium manganese steel deformation behavior using in situ microscopic digital image correlation, in: Materials Science Forum, Vol. 941, Trans Tech Publ, 2019, pp. 198–205.
[30] A. Dutta, D. Ponge, S. Sandlöbes, D. Raabe, Strain partitioning and strain localization in medium manganese steels measured by in situ microscopic digital image correlation, Materialia 5 (2019) 100252.
[31] M. Haupt, A. Dutta, D. Ponge, S. Sandlöbes, M. Nellessen, G. Hirt, Influence of intercritical annealing on microstructure and mechanical properties of a medium manganese steel, Procedia Eng. 207 (2017) 1803–1808.
[32] B. Padmanabhan, P. Salunkhe, D. Nage, Liquid metal embrittlement of austenitic stainless steel fitting caused by copper contamination, J. Fail. Anal. Prev. 15 (4) (2015) 480–485.
[33] W. Savage, E. Nippes, M. Mushala, Liquid metal embrittlement of the heat-affected zone by copper contamination, Weld. J. 57 (8) (1978) 237–245.
[34] W. Savage, E. Nippes, M. Mushala, Copper-contamination cracking in the weld heat-affected zone, Weld. J. 57 (5) (1978) 145s–152s.
[35] R. Haubner, S. Strobl, L.P. Bichler, P. Linhardt, Liquid metal embrittlement of copper brazed plate heat exchangers, Key Eng. Mater. 809 (2019) 535–540.
[36] C. Heiple, W. Bennett, T. Rising, Embrittlement of several stainless steels by liquid copper and liquid braze alloys, Mater. Sci. Eng. 52 (3) (1982) 277–289.
[37] C. Beal, X. Kleber, D. Fabrègue, B. Mohamed, Embrittlement of a zinc coated high manganese TWIP steel, Mater. Sci. Eng.: A 543 (2012) 76–83, http://dx.doi.org/10.1016/j.msea.2012.02.049.
[38] C. Beal, X. Kleber, D. Fabregue, M. Bouzekri, Liquid zinc embrittlement of twinning-induced plasticity steel, Scr. Mater. 66 (12) (2012) 1030–1033.
[39] G. Jung, I.S. Woo, D.W. Suh, S.-J. Kim, Liquid Zn assisted embrittlement of advanced high strength steels with different microstructures, Met. Mater. Int. 22 (2016) 187–195.
[40] H. Kang, L. Cho, C. Lee, B.C. De Cooman, Zn penetration in liquid metal embrittled TWIP steel, Met. Mater. Trans. A 47 (2016) 2885–2905.
[41] R. Autengruber, G. Luckeneder, S. Kolnberger, J. Faderl, A.W. Hassel, Surface and coating analysis of press-hardened hot-dip galvanized steel sheet, Steel Res. Int. 83 (11) (2012) 1005–1011.
[42] J.-H. Kang, D. Kim, D.H. Kim, S.-J. Kim, Fe-Zn reaction and its influence on microcracks during hot tensile deformation of galvanized 22MnB5 steel, Surf. Coat. Technol. 357 (2019) 1069–1075.
[43] C.W. Lee, W.S. Choi, L. Cho, Y.R. Cho, B.C. De Cooman, Liquid-metal-induced embrittlement related microcrack propagation on Zn-coated press hardening steel, ISIJ Int. 55 (1) (2015) 264–271.
[44] O. Dmitrieva, D. Ponge, G. Inden, J. Millán, P. Choi, J. Sietsma, D. Raabe, Chemical gradients across phase boundaries between martensite and austenite in steel studied by atom probe tomography and simulation, Acta Mater. 59 (1) (2011) 364–374.
[45] L. Ripperger, U. Saikia, T. Hickel, K.D. Molodov, S. Sandlöbes-Haut, Influence of Al and Si on Zn induced liquid metal embrittlement in varied steels with and without retained austenite, unpublished, in preparation.